more rapid in the direction of the equatorial oxygens than it is along the vector towards the prism oxygens. This change in the nature of the metal–oxygen interaction with water molecule orientation provides the mechanism for the differential contraction of the bonds to the equatorial and prism waters.

The longer bonds are weaker because there is less overlap between the atomic densities. The weakness of these bonds is reinforced by the repulsive contribution due to polarization of the electron density. This is accompanied by a reduction in strength of the hydrogen bonds linking the ligating waters to the trifluoromethanesulfonate groups, accounting for the tendency for these crystals to lose water at the lutetium end of the series.

All calculations were performed on a Perkin–Elmer 3240 computer using programs from the *XRAY*76 system (Stewart, 1976). This work was supported financially by the Australian Institute of Nuclear Science and Engineering, and by the Research Committee of the Univerity of Western Australia. One of us (AC) gratefully acknowledges receipt of a University Research Studentship.

References

ALBERTSSON, J. & ELDING, I. (1977). *Acta Cryst.* B**33**, 1460–1469.

BACON, G. E. (1975). *Neutron Diffraction*. Oxford: Clarendon Press.

CHATTERJEE, A., MASLEN, E. N. & WATSON, K. J. (1988). *Acta Cryst.* B**44**, 386–395.

ELCOMBE, M. M., COX, G. W., PRYOR, A. W. & MOORE, F. H. (1971). *Programs for the Management and Processing of Neutron Diffraction Data*. AAEC Report TM578. Australian Atomic Energy Commission, Lucas Heights, New South Wales, Australia.

FRENCH, S. & WILSON, K. (1978). *Acta Cryst.* A**34**, 517–525.

GEIER, G. & KARLEN, U. (1971). *Helv. Chim. Acta*, **54**, 135–153.

GEIER, G., KARLEN, U. & ZELEWSKY, A. V. (1969). *Helv. Chim. Acta*, **52**, 1967–1975.

HARROWFIELD, J. M., KEPERT, D. L., PATRICK, J. M. & WHITE, A. H. (1983). *Aust. J. Chem.* **36**, 483–492.

International Tables for X-ray Crystallography (1974). Vol. IV. Birmingham: Kynoch Press. (Present distributor Kluwer Academic Publishers, Dordrecht.)

LARSON, A. C. (1970). *Crystallographic Computing*, edited by F. R. AHMED, pp. 209–213. Copenhagen: Munksgaard.

MELKONIAN, E. (1949). *Phys. Rev.* **76**, 1750–1759.

MEULENAER, J. DE & TOMPA, H. (1965). *Acta Cryst.* **19**, 1014–1018.

MOORE, F. H. (1981). Private communication.

PAIVA SANTOS, C. O., CASTELLANO, E. E., MACHADO, L. C. & VICENTINI, G. (1985). *Inorg. Chim. Acta*, **110**, 83–85.

REUBEN, J. & FIAT, D. (1969). *J. Chem. Phys.* **51**, 4909–4917.

SPEDDING, F. H., PIKAL, M. J. & AYRES, B. O. (1966). *J. Phys. Chem.* **70**, 2440–2449.

STEWART, J. M. (1976). The *XRAY*76 system. Tech. Rep. TR-446. Computer Science Centre, Univ. of Maryland, College Park, Maryland, USA.

STEWART, R. F., DAVIDSON, E. R. & SIMPSON, W. T. (1965). *J. Chem. Phys.* **42**, 3175–3187.

Acta Cryst. (1988). B**44**, 386–395

Electron Densities in Crystals of Nonaaqualanthanoid(III) Tris(trifluoromethanesulfonates)

BY A. CHATTERJEE, E. N. MASLEN AND K. J. WATSON

Department of Physics, University of Western Australia, Nedlands, Australia 6009

(*Received* 12 *May* 1986; *accepted* 12 *February* 1988)

Abstract

The deformation electron densities in crystals of the title compounds for Ln = La, Ce, Pr, Nd, Sm, Eu, Gd, Tb, Dy, Yb and Lu were evaluated using X-ray diffraction data measured at room temperature. The deformation density maps for the lanthanum, gadolinium and lutetium complexes are topologically consistent with those of the neighbouring members of the series. That is, the spherical symmetry of the prepared state for the La^{3+}, Gd^{3+} and Lu^{3+} ions is not preserved in the bonded complexes. For the lighter members, the deformation densities exhibit a symmetric component with excess electron density near each rare-earth nucleus which could be associated with a degenerate form of *f*–*f* orbital product. This disappears at the lutetium end of the series, consistent with its being forbidden by Fermi–Dirac statistics. Close to all rare-earth nuclei there is a strong tricontadipole deformation density component which increases in magnitude with the number of 4*f* electrons. This feature can be accounted for by a 4*f*–5*d* contribution to the density. The effect of anharmonicity on the deformation densities is negligible, as indicated by the radial dependence of the principal features, and confirmed by a neutron diffraction experiment for the neodymium complex. Smaller features further from the rare-earth nuclei occur consistently in all maps for the complexes

0108-7681/88/040386-10$03.00

with the metals from lanthanum to dysprosium. Spiral-shaped components of those densities cannot be described efficiently by separable products of radial and angular functions.

Introduction

The residual electron-density distributions associated with *d* electrons in crystalline materials have been widely studied since the pioneering work on cobalt complexes by Iwata & Saito (1973). The effect of varying the number of 3*d* electrons has been investigated in the γ-M_2SiO_4 structures, with M = Ni, Co, Fe (Marumo, Isobe, Saito, Yagi & Akimoto, 1974; Marumo, Isobe & Akimoto, 1977). Where there are few electrons in the 3*d* subshell the distribution is rather diffuse and covalent bonding is possible. As the subshell is filled the density contracts, and the 3*d* electrons participate less directly in chemical bonding. So far it has not been possible to study all the elements of the first transition series in a single set of isomorphous structures.

The 4*f* electrons in the rare-earth elements are buried more deeply in the atom than are the 3*d* electrons in the elements of the first transition series. It has been suggested that these 4*f* electrons, being shielded by electrons with higher principal quantum number, participate minimally in chemical bonding. Although the structural and magnetic properties of rare-earth compounds are fairly well established, the properties of the 4*f* electrons and the charge density distribution in the vicinity of the rare-earth metals in crystals of these compounds have not yet been examined in detail.

Single crystals of the nonaaqualanthanoid(III) tris-(trifluoromethanesulfonates) form an isomorphous series in which all of the rare earths can be substituted. In the preceding paper (Chatterjee, Maslen & Watson, 1988) the measurement of X-ray diffraction data for the La, Ce, Pr, Nd, Sm, Eu, Gd, Tb, Dy, Yb and Lu members of the series, and neutron diffraction data for the Nd complex, was described.

Deformation densities

In the crystal structures the rare-earth ion in each $[Ln(H_2O)_9]^{3+}$ moiety lies on a $\bar{6}$ axis and is coordinated to the O atoms of nine water molecules situated at the vertices of a tricapped trigonal prism. The hydrated complex ion as a whole has $\bar{6}$ symmetry, with the rare-earth and three symmetry-related O atoms lying in the equatorial plane. The remaining six O atoms at the corners of the trigonal prism are related by either the threefold axis or the equatorial mirror plane.

Sections of the deformation electron density for planes parallel to and 0·0, 0·3 and 0·6 Å from the equatorial plane, and a perpendicular section containing the metal and two symmetry-related prism oxygens were evaluated. A subset of these is reproduced in Fig. 1. The section through the equatorial plane contains the maximum and minimum values of $\Delta\rho$ for each complex.

In order to provide a uniform basis for comparison the scale factor for the observed structure amplitudes for each compound was set at a value k_o such that the magnitude of the deformation density at the metal position is zero. The ratio r of this scale factor to the least-squares value k_l, and the ratio of the difference $k_o - k_l$ to the least-squares standard deviation $\sigma(k_l)$, are listed in Table 1. The values of r for the Pr, Nd and Tb data, which had few outliers in the comparison of symmetry-equivalent intensities, are close to the weighted mean value and none of the others differs significantly from the mean.

The values of k_l are consistently less than the corresponding k_o for all members of the series. This suggests that in the compounds studied there is a deficiency of electron density compared with that in the corresponding free atom within a small sphere of radius ~0·3 Å centred on the rare-earth nucleus. While it is possible that this result is due to systematic bias arising from an inadequacy in the structural model unrelated to the deformation density, or that it arises as an artifact in the least-squares refinement method itself, it is clearly not a manifestation of accumulated random data errors. Typical sections of the deformation density maps obtained with the least-squares scale factor are plotted in Fig. 2. $\sigma(\rho)$, the standard derivation in the electron density, is of the order of 0·1 e Å^{-3} for all maps. This statistic is provided for the benefit of those who believe this to be a useful guide to the reliability of the maps – a view which is not shared by the authors. The consistency of the features, which gives a better guide to reliability, is discussed below.

The extent to which anharmonic thermal motion affects deformation density maps derived from X-ray diffraction data is a matter for concern in charge density analysis. Prominent features may occur if there is anharmonicity which is not allowed for in the structural model. Sections of the neutron diffraction difference density for the neodymium complex are almost featureless in the vicinity of the neodymium nucleus. This indicates that the effect of anharmonicity on the neodymium triflate electron density is small. The similarity of the metal temperature factors for the lanthanum to the dysprosium members of the series [see Table 2 of Chatterjee *et al.* (1988)] suggests that the effects of anharmonicity are not significant for any of these compounds. This is confirmed by the distance of the principal maxima and minima from the nuclear positions in Fig. 1 (*ca* 0·6 Å), which is larger than the value of 0·2 Å expected for anharmonic motion.

X–*N* deformation maps for the neodymium complex were evaluated using the X-ray structural parameters for neodymium with the appropriate neutron parameters for the H, C, O and F atoms. These maps contain

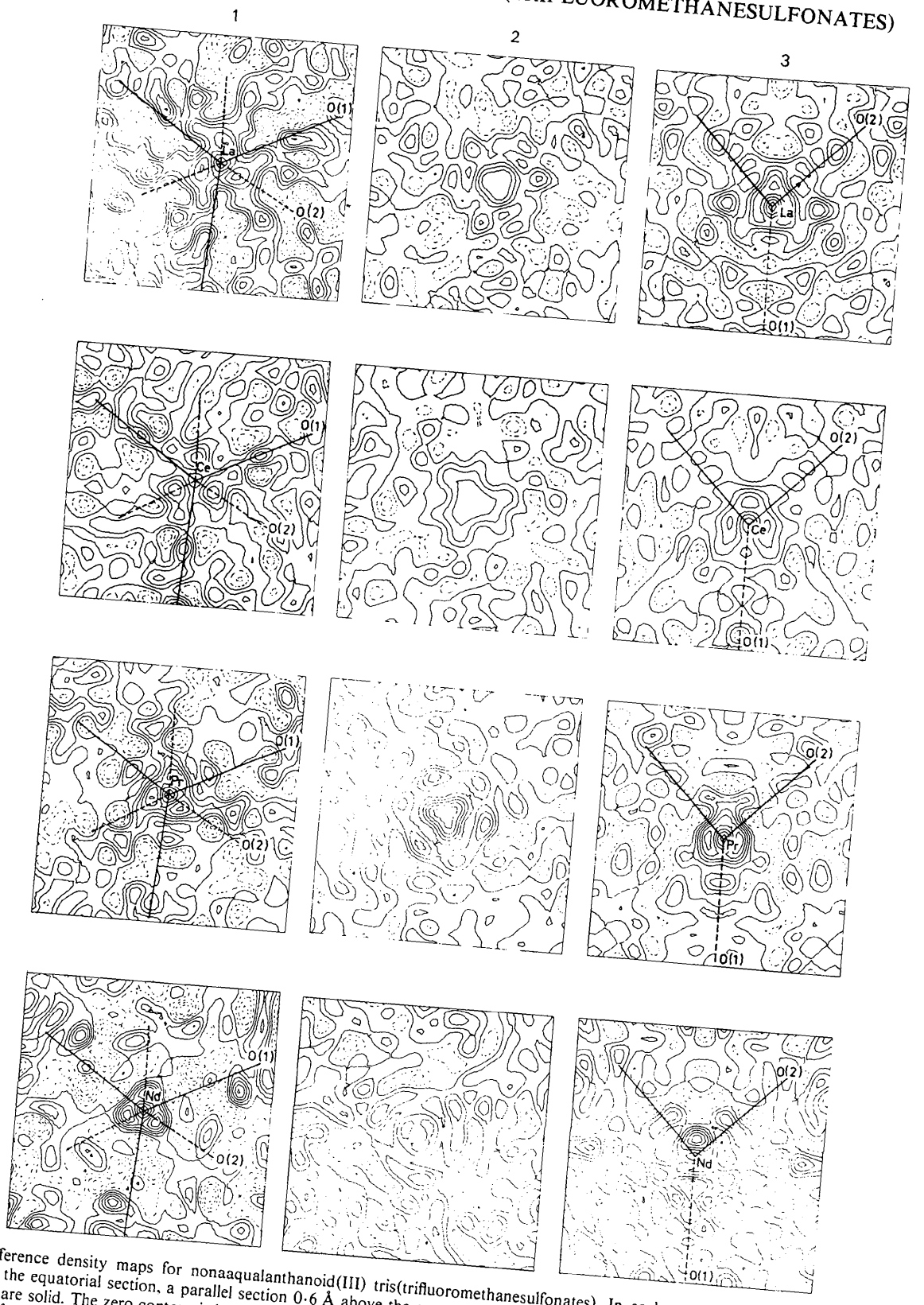

Fig. 1. Difference density maps for nonaaqualanthanoid(III) tris(trifluoromethanesulfonates). In each case column index, $j = 1, 2, 3$, identifies the equatorial section, a parallel section 0·6 Å above the equatorial plane and the perpendicular section respectively. Positive contours are solid. The zero contour is broken. Negative contours are dotted. Contour intervals: rows La to Dy 0·2 e Å^{-3}, rows Yb and Lu 0·4 e Å^{-3}. Map area 5·4 Å^2. In-plane bonds are shown as solid heavy lines, out-of-plane bonds as dashed lines.

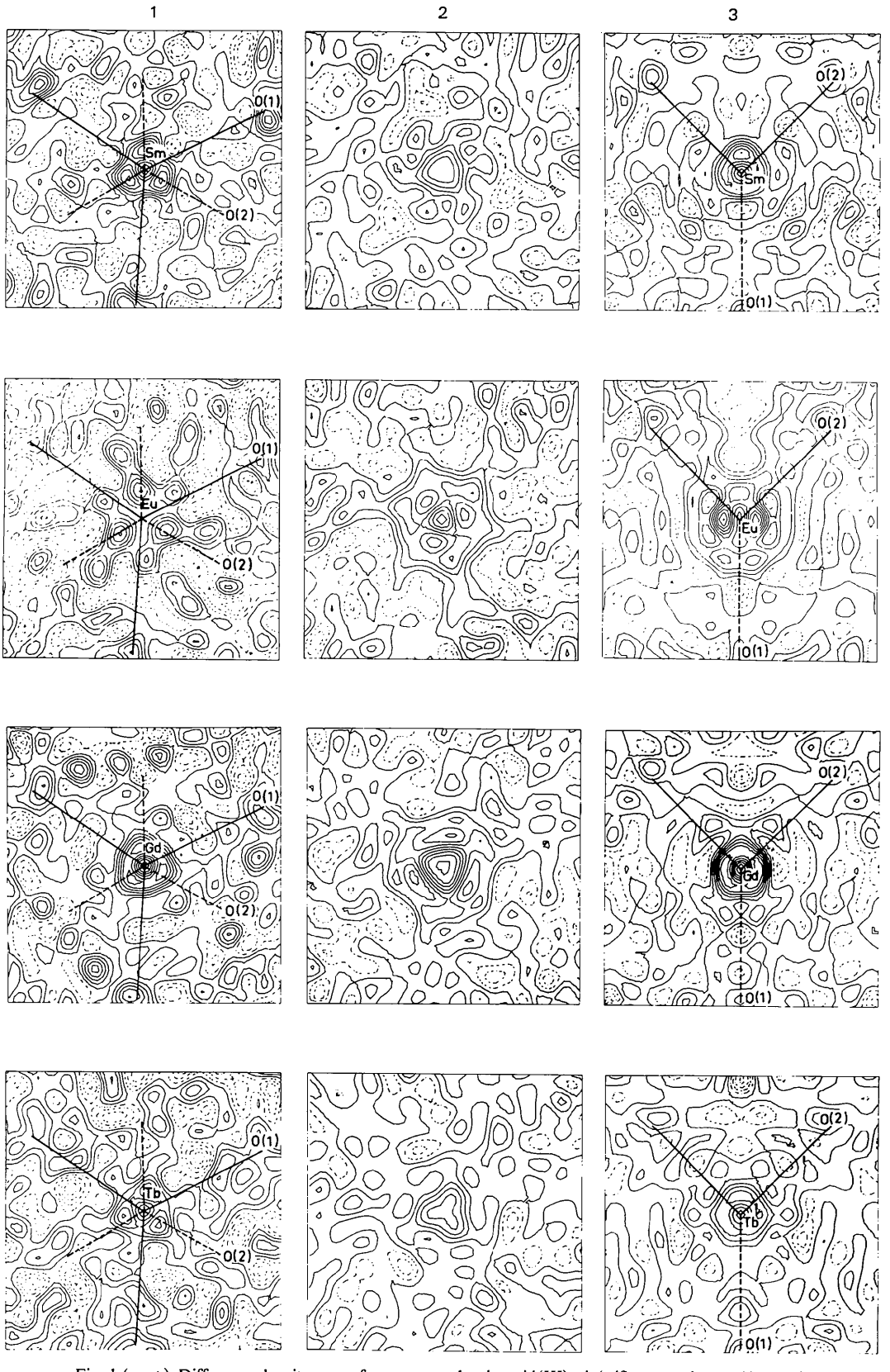

Fig. 1 (*cont.*). Difference density maps for nonaaqualanthanoid(III) tris(trifluoromethanesulfonates).

additional features near the O atoms which can be associated with their lone pairs. The features in the vicinity of the metal atom do not differ significantly from those for the corresponding maps in Fig. 1. Consequently they are not reproduced here.

In all deformation electron-density maps (Fig. 1) there are regions of excess density between the metal–water oxygen vectors. For each complex cation three of these, related by symmetry, have their maxima approximately 0·6 Å from the metal, in the equatorial plane and collinear with the metal–equatorial oxygen vector, but on the side of the metal remote from that oxygen. Two other regions, also related by symmetry, have maxima on the symmetry axis through the lanthanoid ion and approximately 0·6 Å above and below the equatorial plane. On close inspection these regions are seen to be rather diffuse and extended approximately parallel to the equatorial plane. Although not immediately obvious from Fig. 1, when all maps are studied in detail, it appears that each of these regions results from three symmetry-related, unresolved peaks with maxima a short distance from the unique axis. Their densities overlap, yielding an electron-density maximum on the axis. If viewed down the threefold axis these peaks are orientated in a staggered sense relative to the maxima in the equatorial

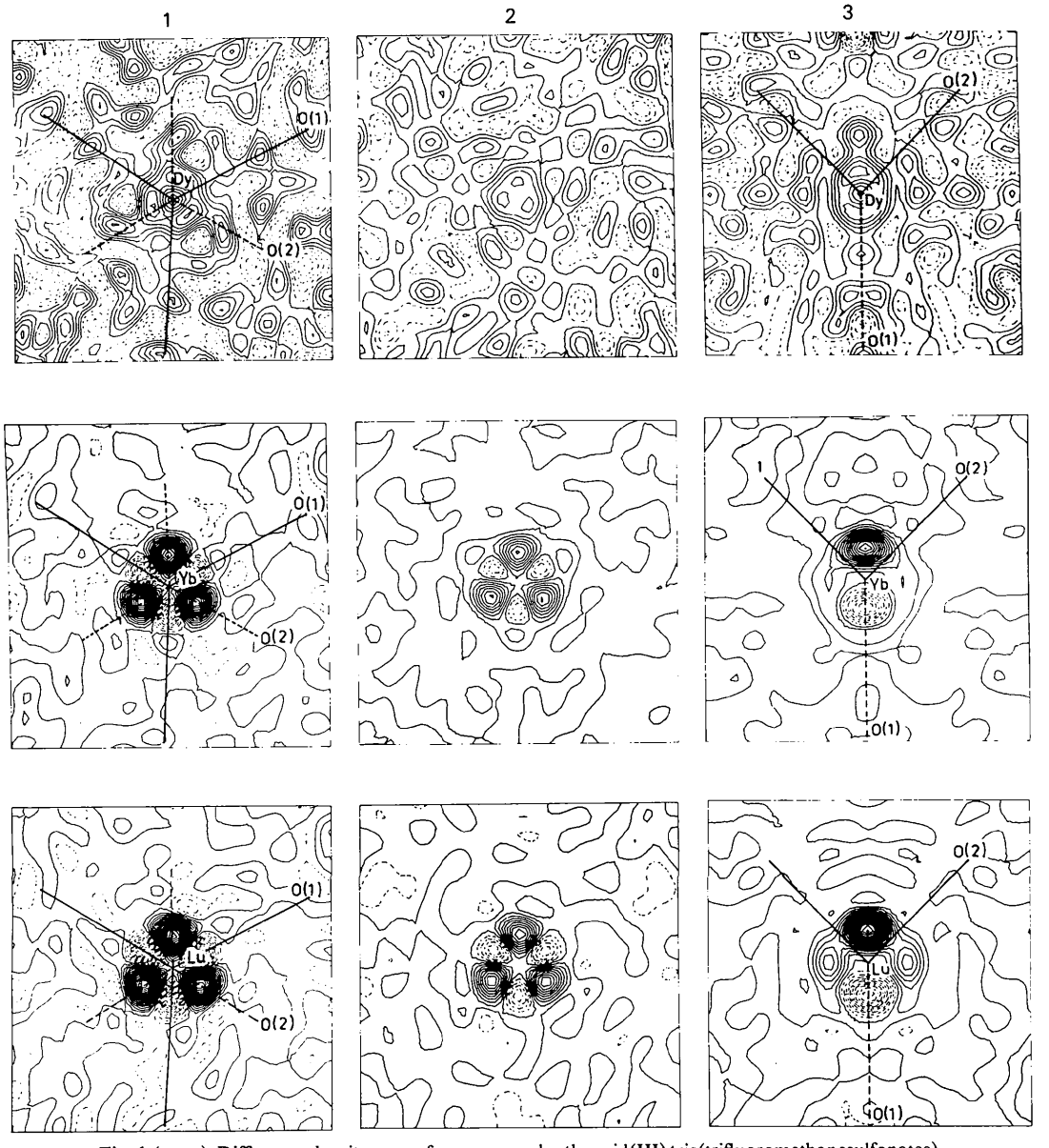

Fig. 1 (*cont.*). Difference density maps for nonaaqualanthanoid(III) tris(trifluoromethanesulfonates).

Table 1. *Comparison of scale factors obtained from the least-squares refinements and those used for the deformation densities of the lanthanoid triflates*

k_l = least-squares scale factor applied on F_o; k_o = scale factor that makes $\Delta\rho = 0$ at the metal site; $r = k_o/k_l$; $\Delta k = k_o - k_l$.

	k_l	$\sigma(k_l)$	k_o	r	$\Delta k/\sigma(k_l)$
LATFS	0·22727	0·00602	0·22813	1·0038	0·143
CETFS	0·25629	0·00535	0·25693	1·0025	0·120
PRTFS	0·27626	0·00394	0·27757	1·0047	0·332
NDTFS	0·36110	0·00299	0·36293	1·0051	0·612
SMTFS	0·29324	0·00392	0·29493	1·0058	0·431
EUTFS	0·34251	0·00405	0·34348	1·0028	0·240
GDTFS	0·27260	0·00448	0·27421	1·0059	0·359
TBTFS	0·38173	0·00311	0·38395	1·0058	0·714
DYTFS	0·39918	0·00243	0·40163	1·0061	1·008
YBTFS	0·18404	0·00910	0·18461	1·0031	0·063
LUTFS	0·19372	0·01252	0·19531	1·0082	0·127
	Mean r			1·0049	
	Weighted mean, w_r			1·0053	
	Standard deviation of r			0·0017	

plane referred to above. There are thus nine electron-density maxima near the lanthanoid ions, disposed with approximate local symmetry $\bar{6}m2$.

At a similar distance (~0·6 Å) from the metal three symmetry-related electron-deficient regions or regions of lesser excess electron density, have minima along the rare-earth–equatorial oxygen vectors. Similarly along the rare-earth–prism oxygen vectors there are regions of a lesser excess electron density within a spherical shell with inner and outer radii approximately 0·4 and 0·6 Å, respectively, from the rare-earth atom. The principal density minima near each metal atom also conform to approximate $\bar{6}m2$ symmetry. As noted above these do not have the characteristics expected of features caused by thermal anharmonicity.

Filled and half-filled subshells

It is sometimes asserted that for compounds containing atoms with filled and half-filled subshells the electron density surrounding such atoms should be spherically symmetric. This is a zeroth-order approximation based on the premise that the deformation density is dominated by the repopulation of near-degenerate orbitals.

Although a featureless deformation density has been reported near an atom with a d^5 configuration in rutile (Shintani, Sato & Saito, 1975), significant deformation

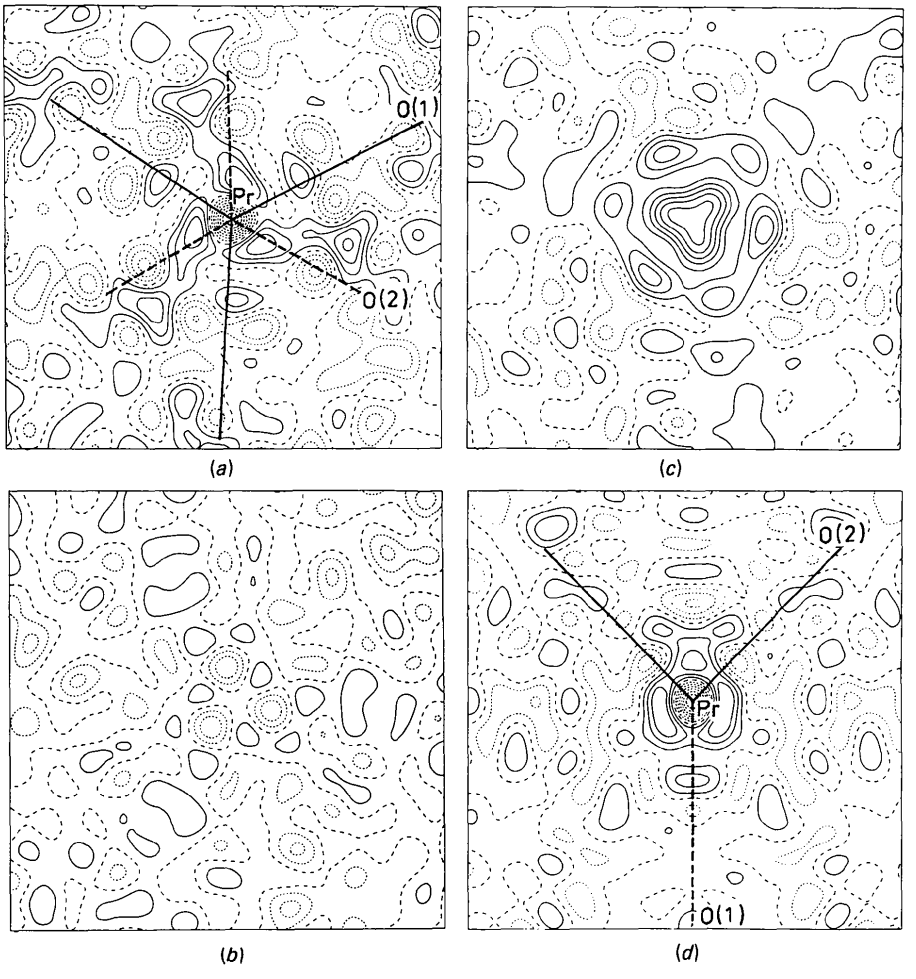

Fig. 2. Difference density maps for the praseodymium member of the series using the least-squares scale factor. (*a*) Equatorial plane, (*b*) 0·3 Å above the equatorial plane, (*c*) 0·6 Å above the equatorial plane, (*d*) section perpendicular to the equatorial plane. Contours and notation as for the Pr maps in Fig. 1.

in d^5 systems was observed by Sasaki, Fujino & Takeuchi (1979) for MnO and by Fujino, Sasaki, Takeuchi & Sadanaga (1981) for γ-Mn_2SiO_4.

If shielding effects were negligible, redistribution of $4f$ electron density due to bonding would indeed be a zeroth-order effect associated with high polarizability. In practice this holds in part only, because electron correlation alters the energies of the repopulated orbitals. The corresponding modifications to the density are field-dependent and must therefore be considered with other field-dependent contributions. All may be regarded as changes to the shapes of the orbitals. For a hydrogen-like atom this effect is of first order, *i.e.* one level higher than prepared-state formation. Hydrogen-like behaviour breaks down as the atomic number increases, because of electron correlation, which increases in importance as the square of the atomic number.

The triply charged ions La^{3+}, Gd^{3+} and Lu^{3+} have the closed-shell xenon core with 0, 7 and 14 f electrons respectively. In all of the corresponding lanthanoid triflates the electron density surrounding the rare-earth atom is not spherically symmetric (although the electron density for the gadolinium member is slightly closer to symmetric than are those of the neighbouring members of the series). Thus the most significant contribution to polarization of the electron density depends, not on the symmetry of the prepared state, but on factors nominally of first order which depend on the strength of the field.

Evidence for orbital interaction with the crystalline field in gadolinium complexes has been obtained by other methods. ESR measurements for gadolinium and the temperature dependence of the crystal-field splitting in single crystals of gadolinium-doped $LaCl_3$ and $LaBr_3$ were studied by Boatner & Abraham (1967). These authors related their studies to the work of Bowden (1966, 1967), who investigated the superhyperfine structure of the ESR spectrum of gadolinium-doped CaF_3 crystals under stress, and reported evidence for an interaction of the $4f$ electrons with the crystal field, which was not predicted by the conventional model of bonding based on a spherically symmetric $4f$ subshell.

In a perturbation expansion treatment of atomic charge density, polarization is described in terms of the population of higher energy levels. As the atomic number increases the energy differences between neighbouring levels decrease for a shielded atom because of the n^{-2} dependence of the energy (n being the principal quantum number). The number of such closely spaced levels increases because of the greater number of angular momentum states which are accessible. The results of these studies indicate that, for the rare-earth elements, polarization with occupation of higher energy levels is more important than repopulation of the $4f$ orbitals. Spherical symmetry for the outer closed subshells is not a useful approximation.

Ce, Pr, Nd, Sm, Tb and Dy triflates

Within 1·2 Å of the metal nucleus the maps in the equatorial planes for members of the series from La to Dy, with the exception of europium triflate, are topologically equivalent in the sense that all have maxima and minima close to corresponding features in the praseodymium map. Since this correspondence involves nine crystallographically independent features on each of nine maps the probability of its occurring by chance is negligible.

The maps in Fig. 1 are not of equal reliability. The refinement indices R and wR, listed in Table 1 of Chatterjee *et al.* (1988), are a guide to accuracy but account must also be taken of the range and strength of the high-angle data. The praseodymium maps were considered to be the most reliable, with the dysprosium and europium being least and second-least reliable for the complexes with fewer than ten f electrons.

The deformation density near the nucleus is closest to $\bar{6}m2$ symmetry. The most significant trend is a strengthening of the features within 0·7 Å of the nucleus with increasing lanthanoid atomic number through the series. It is thus reasonable to associate these features with the metal f electrons.

The $4f$ states of each metal atom are degenerate before bonding. For the corresponding states of a hydrogen-like atom the bonding potential produces a zeroth-order change forming the prepared state ψ_0 (an eigenstate of the bonding term in the Hamiltonian). This gives an approximate description of the behaviour of the many-electron metal atom.

In principle at least, many distinct arrangements of the $4f$ atomic orbital occupancies are possible. To assist in understanding the features near the metal nuclei the 'typical' map in this group was decomposed into symmetric and antisymmetric deformation density components. In general the repopulation of $4f$ orbitals generates symmetric density functions which contain scalar, quadrupole, hexadecapole and hexacontatetrapole components. It is unlikely that the contribution of the highest order pole will be significant because it has too many lobes (64) to accommodate a close-packed array of atoms at normal bonding distances. As expected, the hexacontatetrapole term is not significant.

The symmetric component of the map is dominated by scalar and quadrupole terms with a net positive density – *i.e.* they describe an increase in the f-orbital population.

To understand the origin of the antisymmetric deformation density components requires a study of the deformation terms which are first order in the bonding potential V. The first-order change in the wavefunction is

$$\psi_1 = \sum_{n=0}^{\infty} |\varphi_n\rangle \langle \varphi_n | V | \psi_0 \rangle (E_0 - E_n)^{-1}, \qquad (1)$$

where n ranges over the eigenstates of the Hamiltonian excluding V. E_0 and E_n are the energies for ψ_0 and φ_n respectively. The first-order term in the deformation density is

$$\Delta\rho_1 = \psi_0\psi_1 + \psi_0\psi_1. \qquad (2)$$

For rare-earth atoms the energies for the $5d$, $6s$ and $6p$ states are not far removed from the $4f$ energies (Cowan, 1973, p. 175). Because the denominators of the corresponding terms in (1) are small these make a large contribution to ψ_1. Of these states $5d$ reaches a maximum closest to the nucleus. The matrix elements $\langle\varphi_{5d}|V|\psi_0\rangle$ may be large because of the high degree of overlap of the $4f$ and $5d$ radial functions.

The antisymmetric component of the three-dimensional density near each rare-earth nucleus is characterized by nine maxima alternating with nine minima in approximately $\bar{6}m2$ symmetry. The multipole function with the same angular dependence, shown in Fig. 3, is that of the fifth-order tricontadipole spherical harmonic $P_5^3(\cos\theta)\sin 3\varphi$, where θ and φ are local spherical polar coordinates centred on the rare-earth nucleus and P_l^m is an associated Legendre polynomial. This is the symmetry expected for the $4f$–$5d$ product generated by the $5d$ contribution to ψ_1 (and that of $4f$ to ψ_0).

Outside the region near the rare-earth nucleus the density is more complex and the symmetry is lower. This is also expected since many states with higher principal quantum number contribute in this volume. We focus on the praseodymium maps shown in Fig. 2. In the equatorial plane, secondary features out to 1·2 Å from the metal atom include nine hollows. Three pairs of these are situated with each hollow of a pair either side of, and equidistant from, the rare-earth equatorial oxygen vector, indicating that electrons are redistributed into the bonding region at the expense of the electron-deficient regions either side of the bond. The other symmetry-related hollows lie beyond the higher maxima, on the extension of the equatorial oxygen–rare-earth line. Some excess density also occurs in the lone-pair regions near the equatorial oxygens.

The local symmetry of the deformation density is consistent with the arrangement of the H atoms. Focusing again on Fig. 2, the bonds from O to the two H atoms for each equatorial water molecule, situated above and below the equatorial plane, have an approximate trigonal relationship with the corresponding oxygen–metal vector. The similarity of features either side of the metal–equatorial oxygen vector reflects the symmetrical arrangement of the H atoms and the trigonal geometry about the O atom. There is less indication of pseudosymmetry in the deformation density near the prism oxygen, about which the disposition of bonds is unsymmetrical.

Fig. 2(*a*) contains components of spiral form about 0·8 Å from the nuclei. In the equatorial plane there are maxima radiating outwards from the metal nucleus along three symmetry-related curved arms. The density maximizes in a direction about 18° from the lines of the projections of the Pr—O(2) vectors onto the equatorial plane. This density cannot be described in terms of a limited set of uncorrelated radial and angular functions since the radial and angular variables are non-separable. Because of these non-separable components of the density, the relevance of a description of chemical bonding in terms of limited sets of excited states (orbitals) for these rare-earth complexes must be questioned.

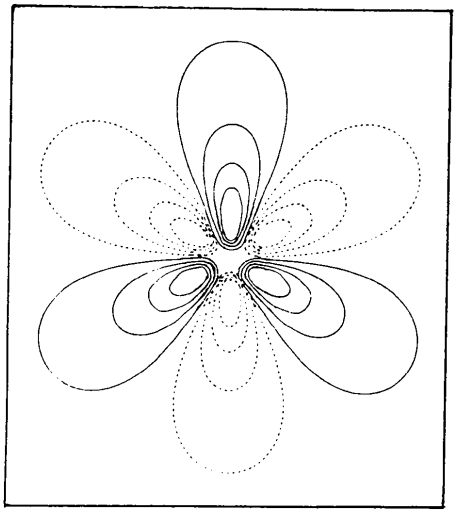

(*a*)

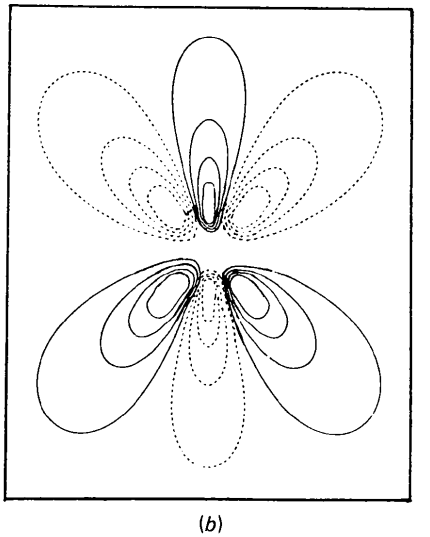

(*b*)

Fig. 3. Contour plot of the function $P_5(\cos\theta)(\sin 3\varphi)r^5\exp(-6r)$. The sections shown are equivalent to (*a*) the equatorial plane and (*b*) the perpendicular plane in the difference densities of the lanthanoid nonahydrate ions. Positive contours solid. Negative contours broken. Uniform contour intervals.

Yb and Lu triflates

The Lu atom contains 14 4*f* electrons – seven with spin 'up' and seven with spin 'down'. The Pauli exclusion principle precludes the 4*f* subshell from accommodating more electrons and consequently of any contribution from an *f*–*f* orbital-product population exceeding two. Hence there cannot be any symmetric *f*–*f* components which make positive contributions to the deformation density.

In the deformation density maps for ytterbium and lutetium triflates the antisymmetric features dominate the deformation density and are relatively stronger in the latter. The symmetric component is small. The change in contour interval from 0·2 to 0·4 e Å^{-3} for these heavier members should be noted (Fig. 1).

Although the orientations of the maxima and minima are similar for the two triflates, the polarization is stronger for the lutetium complex. The symmetry of the idealized deformation density corresponds to a tricontadipole. It is identical in form and orientation to the antisymmetric component of the density near the rare-earth nucleus for each of the other members of the rare-earth series described here. The major features on the equatorial plane maps depart somewhat from the ideal because of particularly strong electron deficiencies along the lines of the metal–equatorial oxygen vectors. The hollows are broadened along the [001] direction, an effect consistent with the shape of the deformation density near trigonally oriented water molecules bonded to a Cu atom in copper sulfate pentahydrate (Varghese & Maslen, 1985).

Although the features in these maps are consistent with the other studies and with expectations from *f*-orbital populations and Fermi–Dirac statistics, consideration must be given to whether those concentrated near the metal nuclei could arise from large anharmonic components in the thermal motion, which is large for both the Yb and Lu crystals. The radial distributions for these features do not support this hypothesis. The maxima and minima in the difference maps are too far from the nuclei. This conclusion is reinforced by an examination of the *hkl* dependence of the Fourier coefficients which contribute to the deformation density. There are a number of low-order reflections, such as 113, for which $|F_{calc.}|$ is markedly less than $|F_{obs.}|$. The intensities of such low-angle reflections are not sensitive to the thermal vibration of the metal atom. This confirms the conclusion that the features in the deformation density are mainly electronic in origin.

On the basis of the perturbation equations (1) and (2) the deformation density will be dominated by a single product when the denominator for one and only one eigenstate φ_n is small. For a triply charged cation beyond lutetium, the 5*d* shell is occupied. Below lutetium it is empty. Thus for lutetium ψ_1 should be dominated by the 5*d* contribution and the corresponding deformation density will consist mainly of the contribution from a 4*f*–5*d* product. That is precisely what is observed.

This perturbation theory argument accounts for the rapid increase in magnitude of the tricontadipole, but does not explain the stronger depletion of density in the equatorial plane, as the 4*f* subshell is filled. It is at first surprising to find deeper hollows associated with the longer metal–oxygen bonds.

Accommodation of the nine ligating water molecules becomes progressively more difficult, owing to the lanthanoid contraction, for the heavier rare-earth metals. The complexes are correspondingly harder to prepare, and the equatorial water molecules are bound less strongly, as indicated by their larger thermal motion and weaker involvement in hydrogen bonding. This trend should be reflected in the deformation density, and indeed the depletion of density along the metal–oxygen bonds is energetically unfavourable. The reduction in binding energy will be partly offset by the increase in electrostatic energy resulting from the decrease of metal–oxygen bond lengths. For the equatorial water molecules that reduction is small, as noted above, so that these waters are weakly bound.

This heavy depletion of electron density near the lone-pair region of the water molecule is accompanied by, and is presumably responsible for, the weakening of the hydrogen-bonding power of the equatorial water molecule. As the strength of the hydrogen bond from this water molecule to the sulfonate O(3) atom diminishes, that from the prism water to O(3) increases to compensate. This is indicated by the changes in lengths of the O–H···O contacts, as described in Chatterjee *et al.* (1988).

For diatomic molecules the free-atom densities in the internuclear region are reduced as the electronegativities of the atoms increase (Spackman & Maslen, 1985). Similar depletion of atomic electron densities is observed in experimental deformation densities containing strongly electronegative first-row atoms (Dunitz, Schweizer & Seiler, 1983). This behaviour is also predicted by the Pauli principle. Likewise, a filled 4*f* subshell cannot accommodate additional contributions to the density from the lone pairs of electron-rich ligands, such as oxygen. Depletion of the 4*f* density, by movement into the 4*d*–5*f* product, is the result. This will clearly be greater for ligating waters with a trigonal orientation, since this maximizes the overlap between the metal *f* shell and the oxygen lone-pair density.

Thus the main topological characteristics of the deformation density for the heavier members of the series can be understood in terms of the Pauli principle and the energy-level structure of the rare-earth series.

This work has been supported financially by the Australian Research Grants Committee, by the

Australian Institute of Nuclear Science and Engineering and by the Research Committee of the University of Western Australia. One of us (AC) gratefully acknowledges receipt of the University Research Studentship.

References

BOATNER, L. A. & ABRAHAM, M. M. (1967). *Phys. Rev.* **163**, 213–219.
BOWDEN, C. M. (1966). *Bull. Am. Phys. Soc.* **11**, 834.
BOWDEN, C. M. (1967). Doctoral Dissertation, Clemson Univ., South Carolina, USA.
CHATTERJEE, A., MASLEN, E. N. & WATSON, K. J. (1988). *Acta Cryst.* B**44**, 381–386.
COWAN, R. D. (1973). *Nucl. Instrum. Methods*, **110**, 173–182.
DUNITZ, J. D., SCHWEIZER, W. B. & SEILER, P. (1983). *Helv. Chim. Acta*, **66**, 123–133.
FUJINO, K., SASAKI, S., TAKEUCHI, Y. & SADANAGA, R. (1981). *Acta Cryst.* B**37**, 513–518.
IWATA, M. & SAITO, Y. (1973). *Acta Cryst.* B**29**, 822–832.
MARUMO, F., ISOBE, M. & AKIMOTO, S. (1977). *Acta Cryst.* B**33**, 713–716.
MARUMO, F., ISOBE, M., SAITO, Y., YAGI, T. & AKIMOTO, S. (1974). *Acta Cryst.* B**30**, 1904–1906.
SASAKI, S., FUJINO, K. & TAKEUCHI, Y. (1979). *Proc. Jpn Acad. Ser. B*, **55**, 43–48.
SHINTANI, H., SATO, S. & SAITO, Y. (1975). *Acta Cryst.* B**31**, 1981–1982.
SPACKMAN, M. A. & MASLEN, E. N. (1985). *Acta Cryst.* A**41**, 347–353.
VARGHESE, J. N. & MASLEN, E. N. (1985). *Acta Cryst.* B**41**, 184–190.

Acta Cryst. (1988). B**44**, 395–406

Crystallography of Systems with Long Periods: a Neutron-Scattering Study of Sodium Dodecyl Sulfate/Water Mesophases

BY P. KÉKICHEFF

Laboratoire de Physique des Solides, associé au CNRS (LA 2), Bâtiment 510, Université de Paris-Sud, 91405 Orsay, France

AND B. CABANE

DPC–SCM–UA 331, CEN Saclay, 91191 Gif-sur-Yvette, France

(*Received 7 July* 1987; *accepted 7 March* 1988)

Abstract

Diffraction patterns are presented for the ordered mesophases of the sodium dodecyl sulfate (SDS)/water lyotropic system. The reciprocal space of the six mesophases has been determined directly through the use of oriented samples. It changes in a nearly continuous way from the most hydrated phase (hexagonal: circular cylinders) to the least hydrated phase (lamellar: bilayers). The orientational behavior of these oriented mesophases has also been used to identify their leading crystallographic planes; this yields an approximate representation of real-space structures. Accordingly, the path from the homogeneously curved cylindrical phase to the flat lamellar phase goes through the production of structures with inhomogeneously curved interfaces (ribbons) or with negative Gaussian curvature (saddle-splay geometry).

1. Introduction

Crystalline arrays of interfaces are formed when amphiphilic molecules (soaps, salts of long chain acids, or other surfactants) are mixed with water in adequate proportions (Ekwall, 1975; Winsor, 1968). These mixtures are liquids because the amphiphilic molecules are in a liquid state, as shown by their wide-angle scattering, where the interferences between neighboring amphiphilic chains show up as a diffuse ring (Luzzati, 1968). These mixtures are also crystals because the array of interfaces is periodic in one, two or three dimensions, as shown by the small-angle scattering where the repetition of interfaces produces sharp diffraction lines (Luzzati, 1968).

The shapes of such interfaces are governed by a set of constraints at the molecular level (Charvolin & Tardieu, 1978). On the one hand, the segregation of polar and apolar groups requires that the separations between interfaces should be of the order of the length of an amphiphilic molecule. On the other hand, the effective forces between the hydrated polar heads (electrical repulsions) and those between the lipidic aliphatic chains (oil–water surface tension) tend to impose a certain value for the curvature of the interfaces. This 'desired' curvature may not be compatible with a radius which is of the order of a molecular length: this is the basic problem behind the shapes of interfaces which has been analyzed in terms

0108-7681/88/040395-12$03.00